Editors' Suggestion

New insights into the formation and growth of boson stars in dark matter halos

Jiajun Chen,[1,*] Xiaolong Du,[2,†] Erik W. Lentz,[1,‡] David J. E. Marsh,[1,§] and Jens C. Niemeyer[1,‖]

[1]*Institut für Astrophysik, Georg-August-Universität Göttingen, Friedrich-Hund-Platz 1, D-37077 Göttingen, Germany*

[2]*Carnegie Observatories, 813 Santa Barbara Street, Pasadena, California 91101, USA*

(Received 10 February 2021; accepted 13 September 2021; published 14 October 2021)

This work studies the formation and growth of boson stars and their surrounding miniclusters by gravitational condensation using nonlinear dynamical numerical methods. Fully dynamical attractive and repulsive self-interactions are also considered for the first time. In the case of pure gravity, we numerically prove that the growth of boson stars inside halos slows down and saturates as has been previously conjectured, and detail its conditions. Self-interactions are included using the Gross-Pitaevskii-Poisson equations. We find that in the case of strong attractive self-interactions the boson stars can become unstable and collapse, in agreement with previous stationary computations. At even stronger coupling, the condensate fragments. Repulsive self-interactions, as expected, promote boson star formation, and lead to solutions with larger radii.

DOI: 10.1103/PhysRevD.104.083022

I. INTRODUCTION

Dark matter (DM) is a hypothetical form of matter, which makes up nearly 27% of the contents in our Universe [1]. A popular idea is that the dark matter could be formed of light (pseudo-)scalar particles with large occupation number so that they can be described by a classical scalar field ϕ, see e.g. [2–8]. The potential of the scalar field can be expanded for small field values as [9–11]

$$V(\phi) = \frac{1}{2}m^2\phi^2 \pm \frac{1}{4!}\frac{m^2}{f_a^2}\phi^4 + \cdots, \tag{1}$$

where m is the particle mass, f_a is the decay constant, and natural units, $\hbar = c = 1$, are used. The plus-minus sign before the ϕ^4 term corresponds to repulsive (+) and attractive (−) self-interaction, respectively. In this paper, we define the dimensional self-coupling constant as $g \equiv \pm\frac{1}{8f_a^2}$. Depending on the detailed models, the particle's mass and coupling constant have different values. For instance, QCD axions have masses in the range 10^{-11}–10^{-2} eV [2,12–23], while the ultralight boson particles have masses as low as 10^{-22}–10^{-19} eV [24–27]. These different parameters can influence gravitational structure formation and the mass distribution of scalar field dark matter in our Universe. For example, for ultralight bosons without self-interaction, their dynamics can be computed in the nonrelativistic regime using the Schrödinger-Poisson (SP) equations. For bosons with repulsive or attractive self-interactions, they have a nonzero self-coupling constant, leading to the Gross-Pitaevskii-Poisson (GPP) equations. Solving the SP or GPP equations, we know that the finite energy ground state solution (for weak self-interactions) of these systems is a soliton: a localized lump of boson energy density held together by the competing forces of gravity, self-interactions, and gradient energy [7,28–30]. Such solitonic solutions are also known as boson stars [11,31–36].

The formation of boson stars has been observed in numerical simulations in a variety of situations relevant to dark matter structure formation [37–42]. The growth rate of boson stars is an important quantity since the more massive and dense stars are easier to observe. Ultimately, if we can understand the masses and abundances of boson stars, then we can predict their observational signatures, in instruments such as haloscopes [43,44] or gravitational waves detectors [45,46], or by gravitational lensing, or via their decay products [47–54].

For bosons without self-interaction, boson stars can form due to gravitational condensation from isotropic initial conditions [40]. After nucleation, boson stars start to acquire mass from the surrounding field, with an initial mass growth rate $\propto t^{1/2}$, as obtained by [40]. However, due to computational limitations,[1] the end-stage evolution of

*jiajun@astro.physik.uni-goettingen.de
†xdu@carnegiescience.edu
‡erik.lentz@uni-goettingen.de
§david.marsh@uni-goettingen.de
‖niemeyer@astro.physik.uni-goettingen.de

[1]The computational costs depend on the size of the system to be simulated. Previous studies such as [40] can only observe the early stage of the growth of boson stars.

 © 2021 American Physical Society

boson stars has yet to be observed despite predictions that saturation of the mass growth rate will drop to $\propto t^{1/8}$ [42]. In fact, if saturation is reached within a Hubble time, the end-stage evolution of boson stars is the main factor determining their mass distribution at present. Thus studying the end-stage evolution of boson stars can help us to search for, and possibly observe, boson stars in the Universe.

Attractive or repulsive self-interaction can further influence the evolution of the boson systems. Dynamical boson star formation in this case has not been studied using nonlinear numerical methods. One example is for QCD axions, where the attractive self-interaction could lead to the collapse of boson stars at a critical mass [55]. Therefore, we need to study the evolution of these kinds of bosons in order to understand mass distribution in our Universe.

Using pseudospectral methods [56], we study the evolution of systems with different scalar potentials. We look at systems that are smaller than previous studies so that we have sufficient resolution to resolve the end-stage evolution of boson stars. We anticipate that our conclusions are also applicable to larger systems. We find the following results in our simulation:

(i) For ultralight bosons without self-interaction, the saturation of boson stars occurs in miniclusters. The mass growth rate of boson stars drops from $\propto t^{1/2}$ to $\propto t^{1/8}$ as conjectured by [42].

(ii) For bosons with attractive self-interaction, such as QCD axions ($10^9 \lesssim f_a \lesssim 10^{12}$ GeV), the self-interaction can cause collapse of boson stars above a critical mass. However, it does not affect condensation and early-stage evolution of boson stars in miniclusters.

(iii) For bosons with a repulsive self-interaction, condensation and growth of boson stars is promoted. At strong coupling, $\rho g^2 \gg 4\pi G m^2$, the resulting boson stars are well described by the Thomas-Fermi profile [57], with a larger radius than the case with no self-interaction (see Appendix C for more details).

(iv) For strong attractive self-interactions which satisfy $\rho g^2 \gg 4\pi G m^2$, e.g. large axion density perturbations generated in early Universe if the Peccei-Quinn symmetry is broken after inflation, the condensate can fragment and form multiple boson stars[2] even in a small simulation box (see also [58] for the case with a saturated scalar potential).

Each of the above results are novel, and have not been found before in the dynamical and nonlinear regime. The observed growth rate of boson stars in our simulations has implications for the expected astrophysical abundance and mass function of boson stars in both the fuzzy DM mass range $m \sim 10^{-22}$–10^{-19} eV, and the QCD axion mass range, $m \sim 10^{-10}$–10^{-2} eV, which we will explore in detail in a future publication. The boson star mass function of fuzzy DM has implications for the cusp-core problem of dwarf spheroidal galaxies (e.g. Ref. [28]), the dynamics of old star clusters (e.g. Refs. [59]), the rotation curves of low surface brightness galaxies (e.g. Ref. [60]), the kinematics in the Milky Way center [61], and possibly for the formation of supermassive black holes [38]. For the QCD axion, the boson star mass function has implications for radio astronomy and other indirect dark matter detection methods [62], in addition to direct detection methods [63]. More generally, a saturation mass of boson stars has implications for gravitational wave searches for exotic compact objects [64], where the saturation mass implies a maximum compactness for boson stars formed by gravitational condensation and accretion.

We start in Sec. II with introducing the GPP equations and our initial distributions. In Sec. III A we study the formation and saturation of boson stars for bosons without self-interaction. In Sec. III B and Sec. III C we study the evolution of bosons with attractive self-interaction and repulsive self-interaction, respectively. In Sec. IV, we study the condensation of multiple fragments. Finally, we present our conclusions in Sec. V. In the Appendixes, we discuss the pseudospectral method, convergence analysis, soliton solutions to the GPP equations, condensation time for gravitational and self-interactions.

II. THE GROSS-PITAEVSKII-POISSON EQUATIONS AND INITIAL DISTRIBUTIONS

In the nonrelativistic, low-density and low-velocity limits, we can rewrite the scalar field ϕ as

$$\phi = \sqrt{\frac{2}{m}}\mathrm{Re}(\psi e^{-imt}). \tag{2}$$

The complex wave function ψ at lowest order satisfies the GPP equations [65,66]

$$i\frac{\partial}{\partial t}\psi = -\frac{1}{2m}\nabla^2\psi + mV\psi + g|\psi|^2\psi, \tag{3}$$

$$\nabla^2 V = 4\pi G m(|\psi|^2 - n), \tag{4}$$

where G is Newton's gravitational constant, V is the gravitational potential, $g \equiv \pm\frac{1}{8f_a^2}$ is the dimensional self-interaction coupling, and n is the mean number density. Examining Eqs. (3) and (4), we find that they are invariant under the scaling transformation

$$\{\mathbf{r}, t, \psi, V, g\} \to \{\lambda^{-1}\mathbf{r}, \lambda^{-2}t, \lambda^2\psi, \lambda^2 V, \lambda^{-2}g\}, \tag{5}$$

where λ is an arbitrary parameter.

Equations (3) and (4) can be written in a dimensionless form following the definitions in Ref. [40]:

[2]Boson stars formed in this regime are unstable and experience runaway collapse.

substitutions $x = \tilde{x}/(mv_0)$, $t = \tilde{t}/(mv_0^2)$, $V = \tilde{V}v_0^2$ and $\psi = \tilde{\psi}v_0^2\sqrt{m/(4\pi G)}$, $g = \tilde{g}4\pi G/v_0^2$, where v_0 is a reference velocity, e.g. the characteristic velocity of the initial state. The dimensionless equations are given by

$$i\frac{\partial}{\partial\tilde{t}}\tilde{\psi} = -\frac{1}{2}\tilde{\nabla}^2\tilde{\psi} + \tilde{V}\tilde{\psi} + \tilde{g}|\tilde{\psi}|^2\tilde{\psi}, \tag{6}$$

$$\tilde{\nabla}^2\tilde{V} = |\tilde{\psi}|^2 - \tilde{n}. \tag{7}$$

We use the wave function momentum distribution [40], $|\psi_{\vec{p}}|^2 = N\delta(|\vec{p}| - mv_0)$ in a periodic box of size L as initial conditions, where $N \equiv nL^3$ is number of nonrelativistic bosons in the box. Performing an inverse Fourier transform on $\psi_{\vec{p}}e^{iS}$ with S a random phase, we obtain an isotropic initial distribution in position space, $\psi(\vec{x}, 0)$. This initial distribution follows from the uncertainty principle: exact knowledge of $\vec{p}$ gives complete uncertainty in $\vec{x}$. The initial wave function is then evolved by solving the GPP equation numerically using pseudospectral method [67,68] (see also in Appendix A). In order to study isolated halos/miniclusters, we run simulations in a box of size $\tilde{L} > 2\pi/\tilde{k}_J$ with $\tilde{k}_J = (4\tilde{n})^{1/4}$ the dimensionless Jeans wave number, since nonrelativistic boson gas forms clumps at scales larger than $2\pi/\tilde{k}_J$ due to Jeans instability [69]. To study the influence of self-interactions, we vary the dimensionless coupling constant $\tilde{g}$ within the range $[-10^2, 10^{-2}]$. Note that $\tilde{g}$ is related to the decay constant by

$$|\tilde{g}| = \frac{v_0^2}{4\pi G}\frac{1}{8f_a^2} = 1.5\times10^{-6}\left(\frac{v_0}{3\times10^{-5}\ \mathrm{km/s}}\right)^2\left(\frac{10^{11}\ \mathrm{GeV}}{f_a}\right)^2. \tag{8}$$

For a given f_a, the value of $\tilde{g}$ depends on the reference velocity one chooses. So to compare $\tilde{g}$ in different systems, we should choose the reference velocity to be the characterized velocity of the system.

III. CONDENSATION OF BOSONS

A. Condensation of bosons without self-interactions

For bosons without self-interactions ($\tilde{g} = 0$), the GPP equations can be simplified as SP equations:

$$i\frac{\partial}{\partial\tilde{t}}\tilde{\psi} = -\frac{1}{2}\tilde{\nabla}^2\tilde{\psi} + \tilde{V}\tilde{\psi}, \tag{9}$$

$$\tilde{\nabla}^2\tilde{V} = |\tilde{\psi}|^2 - \tilde{n}. \tag{10}$$

It has been observed that gravity leads to the formation of a gravitationally virialized DM halo (for certain cosmologies called a "minicluster"), and eventually to the condensation of a boson star at its center [40]. The condensation time, τ_{gravity}, can be derived from the theory of relaxation in the SP equations and the Landau equation [38,40,70], which is given in terms of the radius of miniclusters, R, characteristic velocity, v, and density, n, of the minicluster [40]:

$$\tau_{\mathrm{gravity}} = \frac{b\sqrt{2}}{12\pi^3}\frac{mv^6}{G^2n^2\Lambda} \sim 10^6\ \mathrm{yr}\left(\frac{m}{10^{-22}\ \mathrm{eV}}\right)^3\left(\frac{v}{30\ \mathrm{km/s}}\right)^6 \times\left(\frac{0.1\ M_\odot\,\mathrm{pc}^{-3}}{\rho}\right)^2, \tag{11}$$

where $\Lambda = \log(mvR)$ is the Coulomb logarithm, and b is an $\mathcal{O}(1)$ coefficient to be determined by simulation. After condensation, boson stars have been shown to acquire mass from the surrounding gas of particles, with the subsequent growth rate [40],

$$M_*(t) \simeq M_{*,0}\left(\frac{t - \tau_{\mathrm{gravity}}}{\tau_{\mathrm{gravity}}}\right)^{1/2}, \tag{12}$$

where M_* is the mass of the boson star, and the coefficient $M_{*,0}$ is given by [40]

$$M_{*,0} = (3\pm0.7)\times\frac{v}{4\pi Gm} = (3\pm0.7)\times10^7\ M_\odot\left(\frac{v}{30\ \mathrm{km/s}}\right)\left(\frac{10^{-22}\ \mathrm{eV}}{m}\right). \tag{13}$$

The question arises as to whether the growth in Eq. (12) continues forever or saturates. We know immediately after a boson star has been formed, its growth rate is in accordance with Eq. (12). As this boson star grows, surrounding bosons become gravitationally bound to it in a halo or atmosphere (the minicluster surrounding the star). The halo surrounding the boson star contains granular structure on the scale of the de Broglie wavelength, which can be modeled as consisting of transient "quasiparticles" [29,38]. As the boson star grows in mass, its radius contracts. At a particular mass, $M_{*,\mathrm{sat}}$, the size of the boson star will be of order that of the granular structure. At this time, it has been conjectured that the hot atmosphere will reach virial equilibrium with the star, causing the mass growth to slow down [42]. The transition has been predicted to occur at $v_{\mathrm{vir}^*} \approx v_{\mathrm{halo}}$ [42], where v_{vir^*} and v_{halo} are the viral velocity of the boson star and minicluster respectively. We call this time the saturation time, τ_{sat}. The saturation time is estimated by considering the viral velocity in the gravitational potential of the soliton given by [29]

$$v_{\mathrm{vir}^*}(M_*) = GM_*mw_0^{1/2}, \tag{14}$$

where $w_0 = 0.10851$. Exploiting that $(M_{*,\mathrm{sat}}/v_{\mathrm{vir}*,\mathrm{sat}})^{3/4} = (mGw_0^{1/2})^{-3/4}$, and combining this with Eq. (12) gives

$$M_*(t) \simeq (M_{*,\mathrm{sat}}^3 M_{*,0})^{1/4} \left(\frac{t-\tau_{\mathrm{gravity}}}{\tau_{\mathrm{gravity}}}\right)^{1/8}, \quad (15)$$

where $M_{*,\mathrm{sat}}$ is the boson star mass at the saturation time and $v_{\mathrm{vir}*,\mathrm{sat}} \approx v_{\mathrm{halo}}$. Comparing with Eq. (13), we find that $M_{*,\mathrm{sat}} \sim M_{*,0}$. From Eq. (15), we can estimate the saturation time:

$$\tau_{\mathrm{sat}} = \left[\left(\frac{v_{\mathrm{halo}}}{GmM_{*,0}}\right)^2 \frac{1}{w_0} + 1\right] \tau_{\mathrm{gravity}} \approx 2\tau_{\mathrm{gravity}}. \quad (16)$$

This suggests that the growth of boson star in the center of a minicluster saturates in about one condensation time after its formation.

Due to computational limitations, the prediction of the saturation of boson stars has not been verified [40,42]. In the rest of this subsection, by running a large number of numerical simulations past the estimated saturation time $t > \tau_{\mathrm{sat}}$, we are able to demonstrate that the growth of boson stars in miniclusters indeed saturates as predicted.

We show the evolution of boson stars from our simulations with different L and N to statistically verify our results. From the simulations, we obtain the change of energy, the growth rate of boson stars, etc.

1. Condensation of boson stars

Numerically solving the SP equations at box size $10 < \tilde{L} < 30$ and total mass $500 < \tilde{N} < 1800$, we observe the formation of a boson star and its surrounding halo/minicluster. One example is shown in Fig. 1: box size $\tilde{L} = 18$ and total mass $\tilde{N} = 1005.3$. We can see a minicluster forming gradually from $\tilde{t} \approx 10$ to $\tilde{t} \approx 30$. After that, a dense and nearly spherically symmetric object appears and grows in the center of the minicluster. We find that the radial density profile of the minicluster from this most dense point coincides with the density profile of a soliton solution at $0 < \tilde{r} < 1$ (soliton density profiles are described in Appendix C), and a power law at $\tilde{r} > 1$ (see Fig. 2). We also find that there is always one, and only one, boson star formed in each minicluster. The region outside the boson star has a radial density profile consistent with cold DM on scales larger than the de Broglie wavelength, and with granular structure below it. These results are fully consistent with results of Refs. [38,40,42].

If we restore the physical units of the above dimensionless simulation, e.g. for typical QCD axion with $m \sim 10^{-5}$ eV, it will correspond to an axion minicluster with a mass of $\sim 3.2 \times 10^{-14}\, M_\odot$ and a radius of 5.1×10^5 km. The axion star formed in the center of the minicluster will have a mass of $\sim 5 \times 10^{-15}\, M_\odot$ and a radius of 3.2×10^4 km.

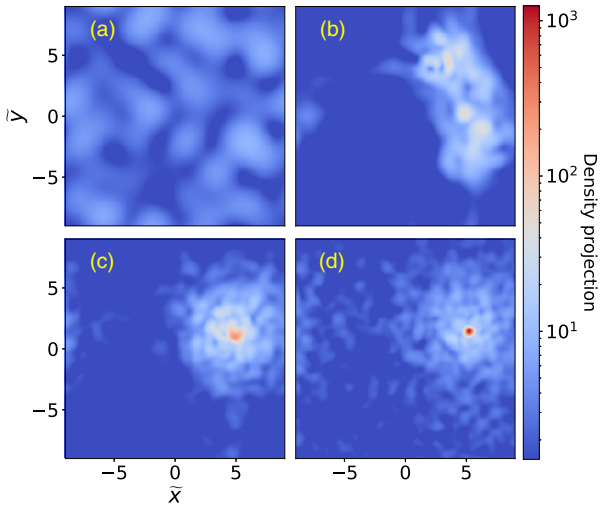

FIG. 1. Snapshots of the density field from one simulation with $\tilde{N} = 1005.3$, $\tilde{L} = 18$. (a) Projected density at the initial time. (b) Projected density at $\tilde{t} = 10$, which shows that minicluster is forming in the box. (c) Projected density at $\tilde{t} = 30$. (d) Projected density at $\tilde{t} = 200$. A single dense object is visible at the center of the minicluster.

2. Growth of boson stars

Figure 3 shows the evolution of mean, normalized, stacked boson star mass for our ensemble of simulations. The boson stars form at $t \approx \tau_{\mathrm{gravity}}$. After that, we find the growth rate of boson star mass $\propto \tilde{t}^{1/2}$ until $t \approx 5\tau_{\mathrm{gravity}}$.

When the size of the boson star becomes smaller than the granular structure in the surrounding halo, the boson star growth saturates and drops to $\propto \tilde{t}^{1/8}$ at the transition time, as predicted by Eq. (15). Therefore, the saturation of boson star growth indeed occurs in our system, and the asymptotic mass growth rate of the boson star matches the theoretical prediction [42]. Note that in Fig. 3 we define τ_{gravity} using

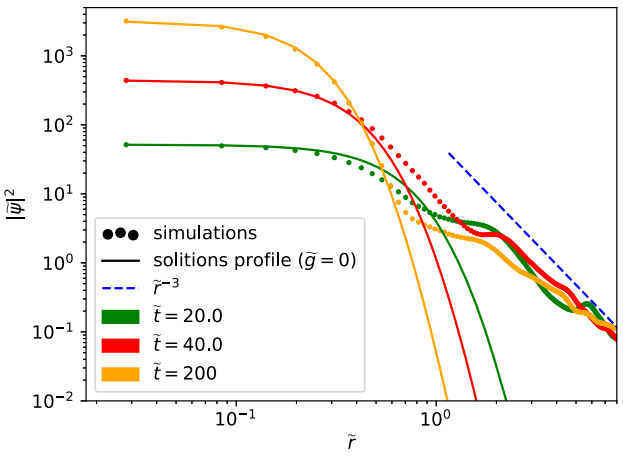

FIG. 2. Density profiles of the minicluster at different times (colored dots) compared with solitonic profiles (solid lines) as given by Eq. (C10) with the same central densities.

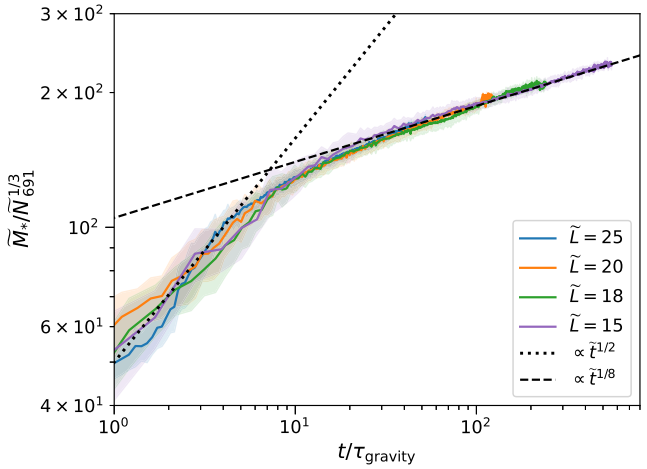

FIG. 3. The mean stacked mass of boson stars evolution (solid lines) for different box sizes $\tilde{L}=25$, 20, 18, 15 and total mass $\tilde{N}=691$, 754, 817, 880, 942, 1005, 1131. The data from simulation with the same box size $\tilde{L}$ but different total mass $\tilde{N}$ are divided into 500 time bins. The shaded regions show the $1-\sigma$ intervals. The time and mass of boson stars are normalized by the condensation time, $\tau_{\rm gravity}$ and the total mass, $\tilde{N}_{691}^{1/3}$, where $\tilde{N}_{691}=\tilde{N}/691$. Note that here $\tau_{\rm gravity}$ is computed using Eq. (11) for the initial configuration, i.e. $R=L$, $v=v_0$, and $n=N/L^3$, to avoid ambiguities in the definitions of halo radius and density.

the characteristic density and velocity of the initial conditions instead of the central density and virial velocity of the minicluster. In reality, the condensation time in the center of minicluster is higher because the characteristic velocity is higher. So the value of saturation time we obtained in units of $\tau_{\rm gravity}$ is a bit larger than the prediction in Eq. (16). Nevertheless, after the formation, the boson star will grow and saturate in $O(1)$ condensation time. Furthermore, we find that during the end stages of evolution, the mass of boson stars can be normalized by $\tilde{N}^\alpha$ with $\alpha\sim0.45$ (for more details, see Appendix D). If we assume the mass of stable halos is proportional to the total mass in the box, $\tilde{N}$, we get the core mass-halo mass relation $M_*\propto M_{\rm halo}^\alpha$. This is broadly consistent with previous findings in cosmological simulations, i.e. $\alpha=1/3$ [38]. In Fig. 3, we choose to normalize the boson star mass by $\tilde{N}^{1/3}$, i.e. assuming the core mass-halo mass relation found by Ref. [38]. Setting α at the best-fit value, 0.45, leads to almost indistinguishable results, and thus we do not show them in Fig. 3. As can be seen, the growth of normalized boson star mass after saturation follows a universal power law.

B. Condensation of bosons with self-interactions

Here we include self-interaction. Self-interactions can promote condensation of bosons. Simulating the GPP equations, we study the evolution of bosons with self-interactions.

1. Bosons with attractive self-interactions

Levkov *et al.* [40] predict that sufficiently weak attractive self-interactions, like those of the QCD axion, have a negligible effect on boson star formation. However, this prediction has not been directly demonstrated.

For bosons with very weak attractive self-interaction, such as QCD axions in minicluster with $v\approx10^{-10}$ [71–73], and decay constant $f_a=1/\sqrt{8|g|}\approx10^{11}$ GeV, we obtain an estimate on the self-interaction coupling of $\tilde{g}\approx-10^{-6}$.

We run some simulations with different $\tilde{g}$. One of these simulations is shown in Fig. 4. We can see the process of formation of the minicluster and condensation of the boson star. This process is similar to the pure gravity case, Fig. 1. The radial density profiles of the minicluster and analytic profiles of soliton with and without self-interactions are given in Fig. 5 and fitted by Eq. (C11) and Eq. (C10), respectively. We discover that the radial density profile of the minicluster coincides with the density profile of a soliton solution at $0<\tilde{r}<1$, with the case with the correct value of $\tilde{g}$ providing a better fit.

The evolution of maximum density from simulations with different strength of self-interactions compared with the case without self-interactions is shown in Fig. 6. These results support the theoretical prediction of [40] that gravity dominates the system and the effect of self-interactions is negligible in the early stages of boson star evolution.

As the central density continues to grow, we can see different trends occur depending on the strength of self-interaction. The growth rate of maximum density still coincides with the case without self-interactions where self-interaction is very weak, e.g. $|\tilde{g}|\sim10^{-6}$. However, if

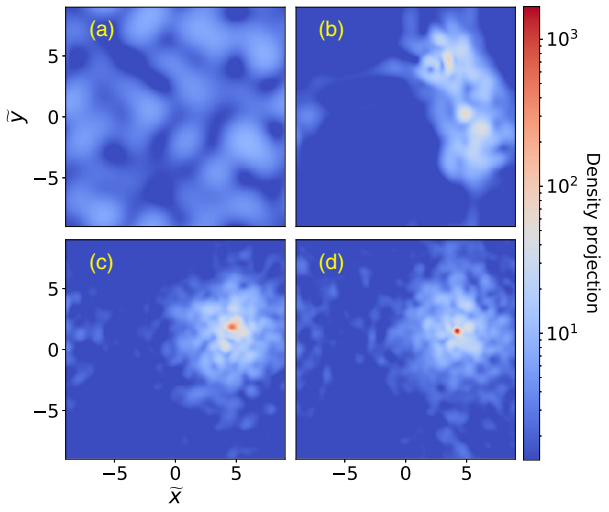

FIG. 4. Snapshots of the density field from one simulation with $\tilde{N}=1005.3$, $\tilde{L}=18$, $\tilde{g}=-0.007$. (a) Projected density at the initial time. (b) Projected density at $\tilde{t}=10$, which shows that minicluster is forming in the box. (c) Projected density at $\tilde{t}=30$. (d) Projected density at $\tilde{t}=48$. Compared with the case without self-interactions, the boson star formed at the center is denser.

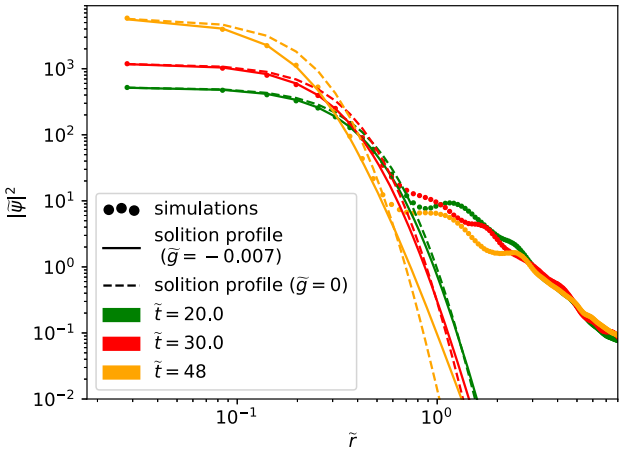

FIG. 5. Density profiles of the minicluster at different times (colored dots) from simulations of the GPP equations with $\tilde{g} = -0.007$. Solitonic profiles given by Eq. (C11) and Eq. (C10) are plotted in solid and dashed lines, respectively.

the self-interaction is moderately weak, e.g. $|\tilde{g}| \sim 10^{-2}$, the effect of self-interactions becomes increasingly important. In the latter case, the boson stars collapse at a critical mass, see Fig. 6 [55,65,74,75]. Above the critical mass, the boson star is unstable to perturbations. The attractive self-interaction in Eq. (3) overcomes the quantum pressure, and boson stars shrink at an accelerated pace, developing huge boson densities in the center when maximum density reaches the critical value, $\sim 0.52/\tilde{g}^2$. Combining the relationship of Eq. (C9), we know the critical mass of collapse is inversely proportional to $\sqrt{\tilde{g}}$, in accordance with the theoretical critical mass, $M_{cr} \propto 1/(m\sqrt{g})$ [65,75] (see also in Appendix C). At the collapse time, the core radius of the

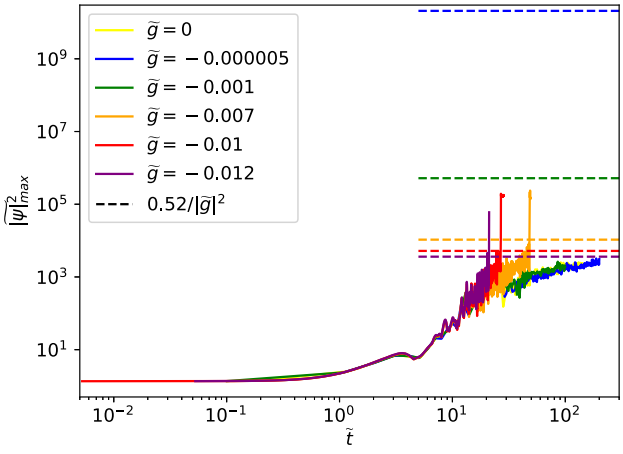

FIG. 6. Maximum density growth with respect to time from simulations assuming different self-interaction couplings: $\tilde{g} = 0$ (without self-interactions), $\tilde{g} = -0.000005$, $\tilde{g} = -0.001$, $\tilde{g} = -0.007$, $\tilde{g} = -0.01$, and $\tilde{g} = -0.012$. The box size $\tilde{L} = 18$ and the total mass $\tilde{N} = 1005.3$. The horizontal dashed lines mark the densities which satisfy $\tilde{\rho}\tilde{g}^2 = 0.52$, when the boson star will collapse.

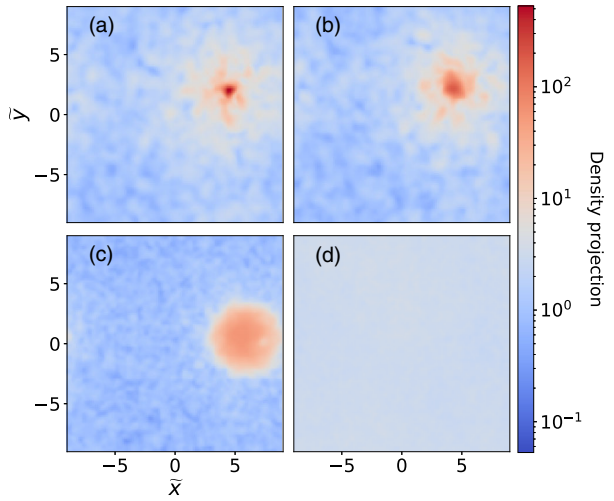

FIG. 7. Snapshots of the density field at $\tilde{t} = 200$ from simulations in a box of size $\tilde{L} = 18$ and total mass $\tilde{N} = 1005.3$ assuming different $\tilde{g}$. (a) $\tilde{g} = 0.01$ (b) $\tilde{g} = 0.1$ (c) $\tilde{g} = 1.0$ (d) $\tilde{g} = 10.0$.

boson star, which is defined as the radius at which the density drops to half of the central density, is given by [see Eq. (C12) for more details]

$$r_{\mathrm{core,cr}} = \frac{1.213}{m f_a \sqrt{32\pi G}} = 291.5\ \mathrm{km} \times \left(\frac{10^{11}\ \mathrm{GeV}}{f_a}\right)\left(\frac{10^{-5}\ \mathrm{eV}}{m}\right). \quad (17)$$

C. Bosons with repulsive self-interactions

In this subsection, we study the evolution of some other candidates for dark matter, bosons with repulsive self-interactions.[3]

By simulating the GPP equations with different positive values of $\tilde{g}$ in a box of size $\tilde{L} = 18$ and total mass $\tilde{N} = 1005.3$, we find miniclusters form and dense objects appear in the center of the miniclusters for sufficiently weak $\tilde{g}$, see Figs. 7(a)–7(c).

The density profiles of the dense objects in the cases with $\tilde{g} = 0.01$ and $\tilde{g} = 0.1$ are shown in Fig. 8, which can be well fit by the density profiles of solitons given by Eq. (C11). Thus, we confirm solitons are condensed in the minicluster. We also prove the kinetic-energy term in Sec. II can be neglected when $\tilde{g} \gtrsim 1.0$ since the density profile of the boson star becomes tantamount to the Thomas-Fermi approximation, Fig. 8. Furthermore, as can be seen in Fig. 7(d), we find that for very large repulsive self-interaction, $\tilde{g} = 10$, no boson star forms at

[3]The linear theory of bosons with repulsive self-interactions, and constraints on the allowed interaction strength of DM, are studied in Ref. [76].

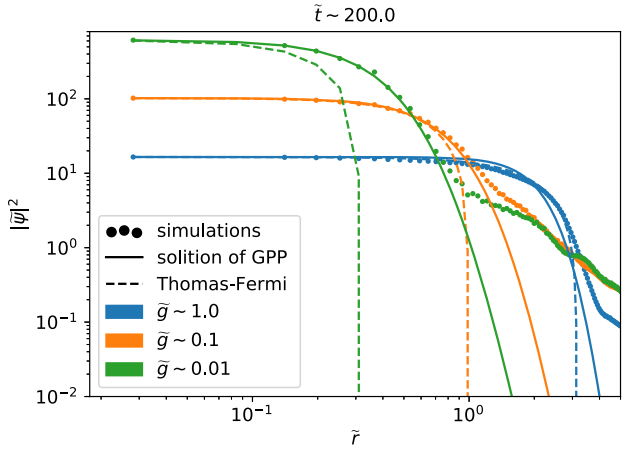

FIG. 8. Density profiles of the miniclusters from simulations (colored dots), compared with solitonic profiles (solid lines) as given by Eq. (C10) and Thomas-Fermi approximation [57] [Eq. (C16)] with the same central densities.

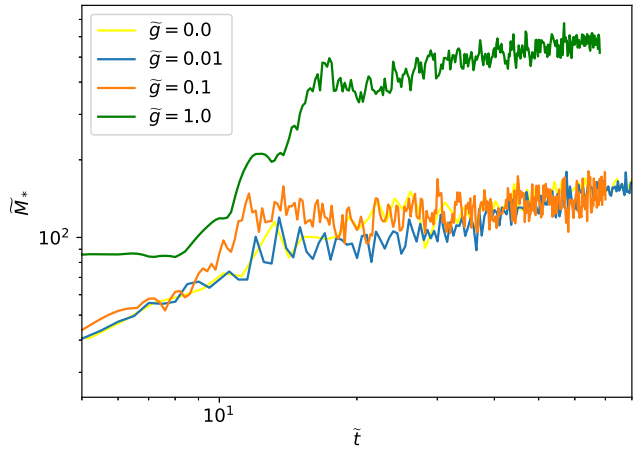

FIG. 10. Mass growth of boson stars with respect to time from simulations assuming different $\tilde{g}$. The box size $\tilde{L} = 18$ and the total mass $\tilde{N} = 1005.3$. Note that the case with $g = 10$ is not shown because no boson star is formed in the box.

all. In this case, the self-interaction dominates over gravity. Due to limited box size, the system forms a uniform condensate instead of a boson star.

The evolution of maximum density with repulsive self-interactions is shown in Fig. 9. The evolution of the maximum density with $\tilde{g} = 0.01$ coincides with the case without self-interaction ($\tilde{g} = 0$) at the early stage. This is similar to the case with weak attractive self-interactions. But at later stages when $\tilde{t} > \tilde{\tau}_{\rm sat}$, the growth rate of the maximum density is different. The growth rate decreases with increasing $\tilde{g}$ as expected.

However, with repulsive self-interactions, the radius of the boson star is larger compared to the case with no self-interactions (see Fig. 8). Thus for boson stars with the same central density, the mass of the ones with repulsive self-interactions is larger. To quantify how many particles condense in different cases, we look at the mass growth of boson stars, Fig. 10. We find that while the central density growth is slower for larger positive g as shown in Fig. 9, the mass growth of boson stars is actually faster with increasing g indicating that repulsive self-interactions promote the condensation process.

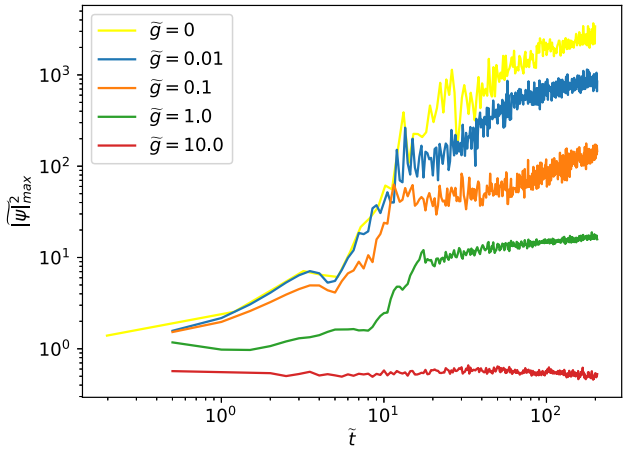

FIG. 9. Maximum density growth with respect to time from simulations assuming different $\tilde{g}$. The box size $\tilde{L} = 18$ and the total mass $\tilde{N} = 1005.3$.

IV. FORMATION OF MULTIPLE BOSON STARS

It is possible that bosons can have even larger values of attractive self-coupling. Thus studying the evolution of these bosons is also necessary. For bosons with attractive self-interactions, we have shown in Sec. III B that when $|\tilde{g}|$ is very small, gravity dominates the early stage evolution in systems and leads to the formation of a single boson star per box.[4] The situation can be very different if $|\tilde{g}|$ is very large, and self-interactions dominate the early stages of evolution [58].

In order to analyze these systems, we first introduce the governing equation for linear overdensity $\delta \equiv \delta\rho/\rho$, where ρ is the mean density. In Fourier space, the linear overdensity δ_k satisfies [74,78,79]

$$\ddot{\delta}_k = -\left(\frac{k^4}{4m^2} + \frac{g\rho k^2}{m^2} - 4\pi G\rho\right)\delta_k. \tag{18}$$

Here we have neglected the Hubble friction term and assumed the cosmic scale factor varies slowly on time scales we are concerned with so that it can be treated as a constant. It is easy to find that δ_k will grow exponentially when

[4]In cosmological simulations [38,60,77], one boson star forms in each halo as it separates out from the cosmic expansion during gravitational collapse. We have verified that this occurs also in our simulations with an expanding background spacetime.

$$k_J^2 < -2\rho g + 2\sqrt{\rho(\rho g^2 + 4\pi G m^2)}, \tag{19}$$

i.e. the growth of the linear perturbation is unstable, thus the overdense regions will quickly undergo nonlinear collapse.

The instability scale k_J is determined by the strength of gravity and self-interactions. For different values of g and ρ, we have three different regimes:

(i) $\rho g^2 \ll 4\pi G m^2$. Gravity dominates, miniclusters form first. After that, one boson star forms in the center of each minicluster.

(ii) $\rho g^2 \approx 4\pi G m^2$. Gravity and self-interactions both play important roles in these regions. A gravitationally bound minicluster may contain multiple boson stars formed from local overdensities.

(iii) $\rho g^2 \gg 4\pi G m^2$. Self-interactions dominate. The condensate can fragment and form multiple boson stars due to self-interactions before a gravitationally bound object forms.

More specifically, different behaviors of the boson stars are determined by the ratio

$$\tilde{\rho}\tilde{g}^2 = \frac{\rho g^2}{4\pi G m^2} = 5.4 \times 10^{-14} \times \frac{\rho}{10^7\ M_\odot/\mathrm{pc}^3} \times \left(\frac{10^{11}\ \mathrm{GeV}}{f_a}\right)^4 \left(\frac{10^{-5}\ \mathrm{eV}}{m}\right)^2. \tag{20}$$

To test this hypothesis, we run simulations with very strong attractive self-couplings. For comparison, we also simulate the Gross-Pitaevskii (GP) equations ignoring gravity:

$$i\frac{\partial}{\partial \tilde{t}}\tilde{\psi} = -\frac{1}{2}\tilde{\nabla}^2\tilde{\psi} + \tilde{g}|\tilde{\psi}|^2\tilde{\psi} \tag{21}$$

under the same initial conditions.

Figure 11 shows the evolution of the system simulated using GPP equations with $\tilde{g} = -0.04$. At the initial time, $\rho g^2/(4\pi G m^2) \sim 3 \times 10^{-4} \ll 4\pi G m^2$. We can see the formation of a minicluster first, Figs. 11(a)–11(c). After that, boson stars form and collapse in the system, see Fig. 11(d). Interestingly, we actually found two boson stars formed in the miniclsuter. This is because the density in the central region of the miniclsuter increases during its formation and at later time ρg^2 becomes comparable with $4\pi G m^2$, i.e. the second regime.

Figures 12(a) and 12(b) show the systems simulated using GPP equations and GP equations with $\tilde{g} = -1.0$, $\rho g^2/(4\pi G m^2) \sim 1$, at $\tilde{t} = 1.0$, We can see two boson stars condense in the dense areas in Fig. 12(a), but not in 12(b), suggesting that the gravity can promote the condensation of boson stars slightly even when self-interactions are strong.

Figures 12(c) and 12(d) show the cases with $\tilde{g} = -80$, $\rho g^2/(4\pi G m^2) \gg 1$. Comparing results from GPP equations with the ones from the GP equations, we do not find a big difference. Therefore, we conclude that the self-interactions dominate the evolution of boson stars alone in some extreme systems.

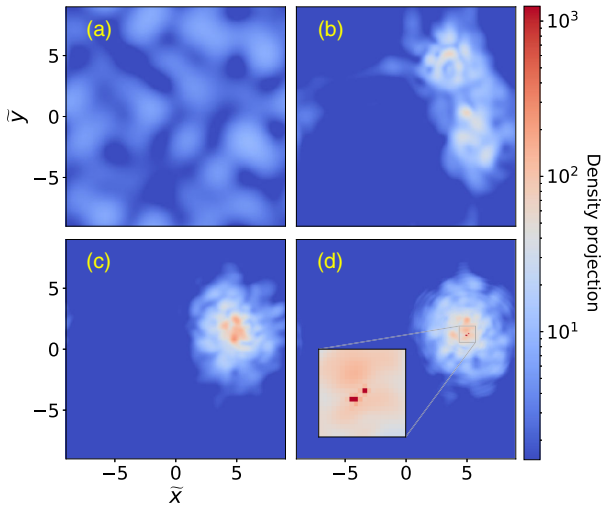

FIG. 11. Snapshots of the density field from simulations of the GPP equations in a box of size $\tilde{L} = 18$, and total mass $\tilde{N} = 1005.3$. The self-interaction coupling constant $\tilde{g} = -0.04$. Note that due to resolution limit, we cannot resolve the central region of the densest object, so we cutoff the projected density in the plot at ≈1500. (a) $\tilde{t} = 0$ (b) $\tilde{t} = 10$ (c) $\tilde{t} = 13$ (d) $\tilde{t} = 13.7$.

In fact, Eq. (E1) suggests the self-interactions can be ignored if $-0.53 \lesssim \tilde{g} < 0$ for a system with box size $\tilde{L} = 18$, total mass $\tilde{N} = 1005.3$, and characteristic velocity $\tilde{v} \sim 1$. But our simulation shows self-interactions are important even for $\tilde{g} = -0.04$ at the late stages of evolution [see Figs. 11(c) and 11(d)]. We think the reason is that at

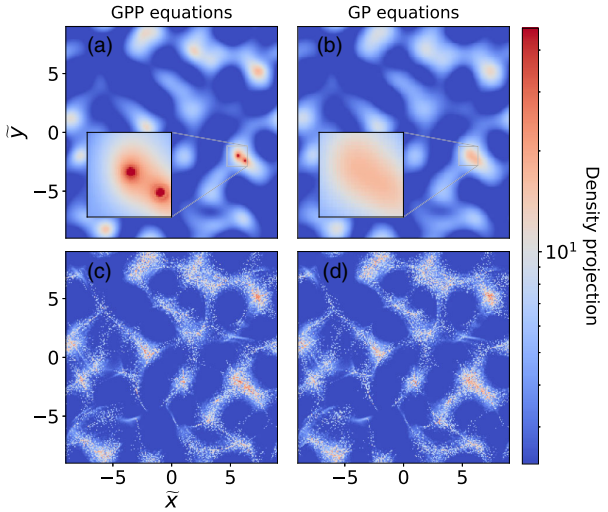

FIG. 12. Snapshots of the density field from simulations of the GPP equations (left column) and GP equations (right column). We pick $\tilde{g} = -1$ (first row) and $\tilde{g} = -80$ (second row). The box size $\tilde{L} = 18$, and the total mass $\tilde{N} = 1005.3$. (a) $\tilde{t} = 1.0$, $\tilde{g} = -1$ (b) $\tilde{t} = 1.0$, $\tilde{g} = -1$ (c) $\tilde{t} = 0.2$, $\tilde{g} = -80$ (d) $\tilde{t} = 0.2$, $\tilde{g} = -80$.

these times, the characteristic velocity increases due to gravitational collapse making the gravitational condensation less efficient. But on the other hand, $\rho g^2/(4\pi m^2 G)$ is larger than the value in the early stage.

In a cosmological setting, the extreme condensate fragmentation observed in our simulations caused by strong self-interactions would spoil the hierarchical nature of cosmic structure formation. However, these results could be applicable to fragmentation of the inflation condensate (e.g. Ref. [80]) or to condensates in condensed matter.

V. CONCLUSIONS

By means of numerical solution of the dynamical Gross-Pitaevskii-Poisson equations, we studied the formation and subsequent growth of boson stars inside gravitationally self-bound halos. We demonstrated a series of new phenomena in the solutions, which had not been seen before in the dynamical regime. Our simulations are local, not cosmological, and so our conclusions apply in all cosmological models that possess the correct environments.

In the case with no self-interactions beyond gravity, we demonstrated the saturation of boson star growth. We ran simulations for times long compared to the dynamical timescales, i.e. $t \gg \tau_{\rm sat} > \tau_{\rm gravity}$, and much longer than those of Ref. [40]. In this regime of boson stars we observed a transition from relatively fast mass growth, $\propto t^{1/2}$, to much slower growth, $\propto t^{1/8}$, in accordance with the prediction made by Ref. [42]. We attribute this to the formation of a gravitationally bound and virialized atmosphere around the boson star, suppressing further mass growth by coupling the condensation time to the boson star's virial temperature.

Another interesting phenomenon is that we discover no significant difference for the end-stage evolution of mass of boson stars (see Fig. 3) normalized by $\tilde{N}^\alpha \propto \tilde{M}^\alpha_{\rm halo}$. The best-fit value of α is 0.45, which is broadly consistent with the core mass-halo mass relation found in previous cosmological simulations, i.e. $\alpha = 1/3$ [38].

In any case, our observation of a reduced boson star growth rate at late times explains why boson stars in virialized halos in cosmological simulations (e.g. Refs. [37,42,77]) are only observed to grow very slowly compared to the other gravitational timescales, and thus populate an almost constant in time core-halo mass relation (see also Ref. [81], which considers the effect of mergers). The saturation of boson star growth will play a role in fixing the cosmological mass function of boson stars formed of axions and ALPs in all cosmological scenarios, although we leave a quantitative study of this to future work.

Our results in the case of attractive self-interactions demonstrated for the first time that boson stars can grow via accretion and reach the critical mass for collapse. Once the critical mass is reached, relativistic simulations are needed. The relativistic simulations of Refs. [11,35] began with supercritical stars, and showed that these stars lead to either ejection of relativistic bosons and a massive remnant (nova) if $f_a \lesssim M_{\rm pl}$, or, for weak self-interactions, $f_a \gtrsim M_{\rm pl}$, collapse to black holes. Our dynamical simulations show that it is possible to reach such critical nova state dynamically before saturation. This implies that such a star could undergo a series of novae in its lifetime. This could have implications for the abundance of relativistic particles in the Universe. If the bosons produced can be converted into visible photons, as is the case for axions and axionlike particles, the nova ejecta could even be observed. We leave for future work the study of he expected rates in realistic models. The regime of weak coupling is applicable to the QCD axion, and so we have demonstrated that such novae could occur for models where the QCD axion composes the dark matter. However, further study is required to determine in which astrophysical environments or cosmologies QCD axion novae are expected to occur in abundance.

In the case of very strong attractive interactions, we demonstrated that these can dominate over gravity and lead to fragmentation of the condensate into many small, dense regions. Such fragmentation has not been seen before in simulations including gravity. This has implications for the fragmentation of the inflaton condensate during the reheating epoch [80,82].

Our results in the case of repulsive interaction demonstrated that such an interaction can promote boson star formation. We showed for the first time that the stable Thomas-Fermi-like solution, which has been studied often in the literature on scalar field DM (e.g. Refs. [57]), can be reached dynamically via gravitational accretion. Repulsive self-interactions change the mass-radius relation of boson stars, and we have shown that these solitons can also be formed dynamically via condensation. A realistic formation mechanism for such states also has implications for the gravitational wave searches for exotic compact objects [64], and could be used to predict the expected signal rates in gravitational wave detectors [83]. Given the sign and strength of the interaction required in this case, the formation of Thomas-Fermi condensates is not applicable to the QCD axion, but could occur in more generalized ALP or scalar field dark matter models with strong attractive self interactions.

In summary, we have demonstrated new results on the dynamical formation and growth of boson stars in a collection of different models, including self-gravity, attractive and repulsive self-interactions. Our results have applications to future terrestrial, astrophysical, and cosmological observations searching for new types of bosons across a wide range of scales.

ACKNOWLEDGMENTS

We thank B. Schwabe, J. H. H. Chan, M. Gosenca, S. Hotchkiss, and R. Easther for helpful discussions. We would also like to thank L. Visinelli, Z. Liu, Z. Chen,

D. Chen, Y. Huo, X. Kong, S. Hoof for constructive comments which helped to improve this paper. X. D. thanks Chanda Prescod-Weinstein for beneficial discussions. D. J. E. M. thanks Luca Visinelli for useful discussions. J. C. acknowledges the China Scholarship Council (CSC) for financial support. X. D. acknowledges support from NASA ATP Grant No. 17-ATP17-0120. D. J. E. M. and E. W. L. are supported by the Alexander von Humboldt Foundation and the German Federal Ministry of Education and Research.

APPENDIX A: PSEUDOSPECTRAL METHOD

To solve the SP, GP, and GPP equations, we use a fourth-order time-splitting pseudospectral solver with GPU acceleration [84]. Compared to the fourth-order pseudospectral method used in [67], our code is 6 to 7 times faster under the same resolution.

The wave function is advanced in time by a unitary operator,

$$\psi(t+\Delta t) = e^{-i\hat{H}\Delta t}\psi = e^{-i(K+W)\Delta t}\psi, \tag{A1}$$

where the Hamiltonian operator is split into the kinetic part K and the potential part W. Δt is the time step size. In general, the operator $e^{-i(K+W)\Delta t}$ can be expanded as

$$e^{-i(K+W)\Delta t} = \prod_j^N (e^{-ik_j\Delta t K} e^{-iv_j\Delta t V}), \tag{A2}$$

where k_j and v_j are constant parameters which are determined by requiring that the expansion is accurate up to a specified order. For example, to the second order, we obtain the well-known leapfrog method,

$$e^{-i(K+W)\Delta t} = e^{-i\frac{1}{2}W\Delta t} e^{-iK\Delta t} e^{-i\frac{1}{2}W\Delta t} + \mathcal{O}(\Delta t^3), \tag{A3}$$

which is also referred to as the "kick-drift-kick scheme." In our simulations, we implement the fourth-order algorithm proposed by [85,86]

$$\begin{aligned} e^{-i(K+W)dt} = &\ldots e^{-iv_0\Delta t W} e^{-it_1\Delta t K} e^{-iv_1\Delta t W} \\ &\times e^{-it_2\Delta t K} e^{-iv_2\Delta t W} + \mathcal{O}(\Delta t^5), \end{aligned} \tag{A4}$$

where v_0, t_1, v_1, t_2, v_2 are parameters, and … means operations symmetric with the right terms in the equation. These parameters are given by

$$w = \sqrt{3 - 12v_1 + 9v_1^2}, \tag{A5}$$

$$t_1 = \frac{1}{2} - t_2, \tag{A6}$$

$$t_2 = \frac{1}{4}\left(1 - \sqrt{\frac{9v_1 - 4 + 2w}{3v_1}}\right), \tag{A7}$$

$$v_0 = 1 - 2(v_1 + v_2), \tag{A8}$$

$$v_1 = \frac{121}{3924}(12 - \sqrt{471}), \tag{A9}$$

$$v_2 = \frac{1}{6} - 4v_1 t_1^2. \tag{A10}$$

For the time step size, Δt, we require [87]

$$\Delta t = \min\left\{\frac{m\Delta x^2}{6\pi}, \frac{\pi}{4mV_{\max}}\right\}, \tag{A11}$$

where $V_{\max}$ is the maximum absolute value of the potential and Δx is spatial cell size.

APPENDIX B: CONVERGENCE ANALYSIS

1. Temporal resolution

To test the convergence of our code in time, we run one typical simulation with decreasing time step sizes and examine the conservation of total energy. The box has a length of 18 on each side and is simulated with 256^3 cells. The bosons in the box have only gravitational interaction, i.e. $\tilde{g} = 0$, and have a total mass of 1005.3. We find that the total energy is fourth-order conserved as expected (see Fig. 13).

2. Spatial resolution

We run the same simulation in Sec. B 1 with different spatial resolutions: 128^3, 256^3, and 512^3. The maximum density in the box as a function of time is shown in Fig. 14. As can be seen, the results from the lowest-resolution run is consistent with the highest-resolution run, suggesting that even with a resolution as low as 128^3. we can already get reliable results.

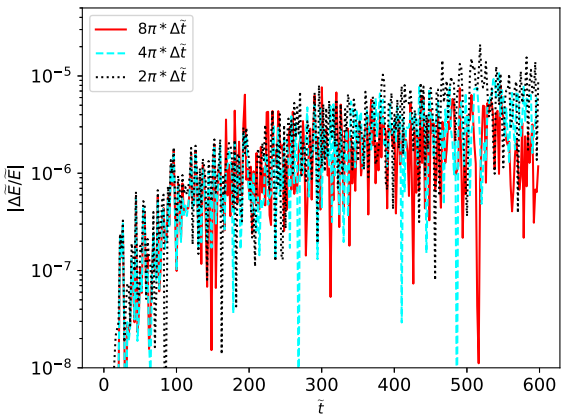

FIG. 13. Relative errors of the total energy with respect to time for different time step sizes. To show the fourth-order convergence of the algorithm in time, we have multiplied the relative errors by a factor of 2^4 and 4^4 for the cases with time step sizes $4\pi\Delta\tilde{t}$ and $2\pi\Delta\tilde{t}$, respectively.

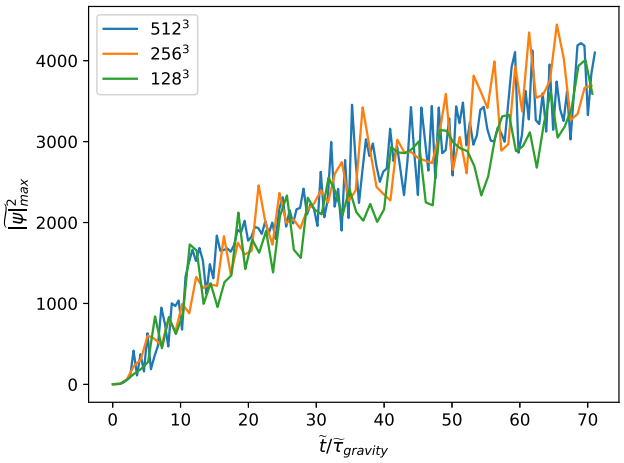

FIG. 14. Maximum density growth with respect to time for spatial resolutions.

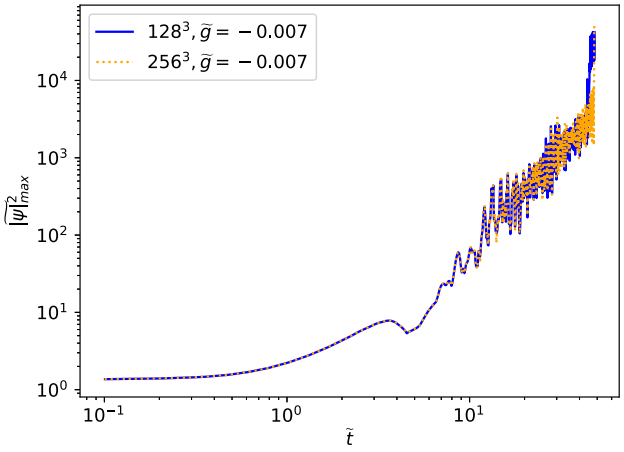

FIG. 15. Maximum density with respect to time for different spatial resolutions. The bosons have attractive self-interaction, i.e. $\tilde{g} = -0.007$.

We also check the cases with self-interactions. The initial conditions are taken to be the same, but the simulations are run with $\tilde{g} = -0.007$. The maximum density is shown in Fig. 15. Again, we can see that the results are converged as the resolution increases. At late times when the central density of the boson star approaches to the critical value, the maximum density has a rapid increase. This happens slightly later in the high-resolution run suggesting that we may not have enough resolution at that time. But in this paper, we will focus on the growth of boson star before the critical collapse.

APPENDIX C: SOLITON SOLUTIONS TO THE GPP EQUATIONS

Plugging the ansatz of stationary solution

$$\psi(\mathbf{r}, t) = \psi(\mathbf{r})e^{-iEt} \tag{C1}$$

into Eqs. (3) and (4), we get the time-independent GPP equations

$$-\frac{1}{2}\nabla^2\psi(\mathbf{r}) = [E - V(\mathbf{r}) - g|\psi(\mathbf{r})|^2]\psi(\mathbf{r}), \tag{C2}$$

$$\nabla^2 V(\mathbf{r}) = |\psi(\mathbf{r})|^2. \tag{C3}$$

Here we have written the equations in dimensionless form as in Sec. II and dropped the tildes over the dimensionless quantities for simplicity. The soliton solution is the eigenstate of Eqs. (C2) and (C3) with the lowest eigenenergy under the boundary conditions

$$\psi(0) = \psi_0, \tag{C4}$$

$$\psi'(0) = 0, \tag{C5}$$

$$\psi(\infty) = 0, \tag{C6}$$

$$V'(0) = 0, \tag{C7}$$

$$V(\infty) = 0. \tag{C8}$$

In practice, Eqs. (C2) and (C3) can be solved numerically using the shooting method: (1) let $V(0) = V_0$, $E = E_0$ and integrate the equations outward from $r = 0$; (2) adjust the values of V_0 and E_0 until the boundary conditions Eqs. (C6) and (C8) are satisfied.

Note that the GPP equations have the following scaling symmetry:

$$\{\mathbf{r}, t, \psi, E, V, g\} \to \{\lambda^{-1}\mathbf{r}, \lambda^{-2}t, \lambda^2\psi, \lambda^2 E, \lambda^2 V, \lambda^{-2}g\}, \tag{C9}$$

where λ is an arbitrary nonzero parameter. Using this scaling symmetry, we can transform one soliton solution to another solution that has a different central density $\rho_0 = |\psi_0|^2$ but the same $g^2\rho_0$.

For a scalar field without self-interaction, i.e. $g = 0$, it has been shown that the density profile of a soliton can be well fit by [28,38]

$$\rho_{\text{soliton}}(r) = \rho_0\left[1 + 0.091\left(\frac{r}{r_{\text{core}}}\right)^2\right]^{-8}. \tag{C10}$$

Here only one of the parameters ρ_0 and r_{core} is independent. Given ρ_0, the core radius, defined as the radius where the density drops to half of the central density, $r_{\text{core}} = 1.308\rho_0^{-1/4}$. The soliton is uniquely determined by its central density.

When the self-interaction is non-negligible, we will need an additional parameter $g^2\rho_0$ to determine the soliton profile.

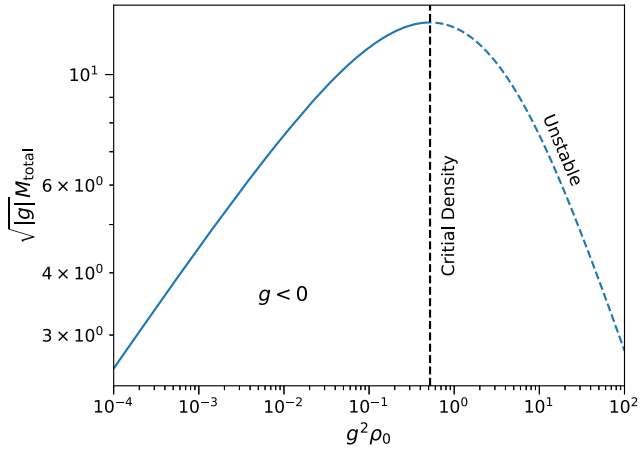

FIG. 16. Total mass of boson star with attractive self-interactions ($g < 0$) as a function of the central density.

As $g^2\rho_0$ approaches 0, we expect that the soliton has the same density profile as Eq. (C10). So we assume in the general case the soliton density profile has a form of

$$\rho_{\rm soliton}(r) = \rho_0\left[1 + (-1 + 2^{1/\beta})\left(\frac{r}{r_{\rm core}}\right)^{\alpha}\right]^{-\beta}, \quad \text{(C11)}$$

where α and β are functions of $g^2\rho_0$ only. When $g\rho_0^2 \to 0$, we require that $\alpha \to 2$, and $\beta \to 8$.

We first consider the case with attractive self-interactions, i.e. $g < 0$. As is well known, there exists a critical mass above which a boson star with attractive self-interactions is unstable [65,74]. In Fig. 16, we show the total mass of the boson star, $\sqrt{|g|}M_{\rm total}$, with respect to its central density, $g^2\rho_0$. As expected, $\sqrt{|g|}M_{\rm total}$ increases with $g^2\rho_0$ and reached a maximum value, 12.72, at $g^2\rho_0 = 0.52$. When the central density increases further, the soliton solution becomes unstable and its total mass decreases as the central density increases.

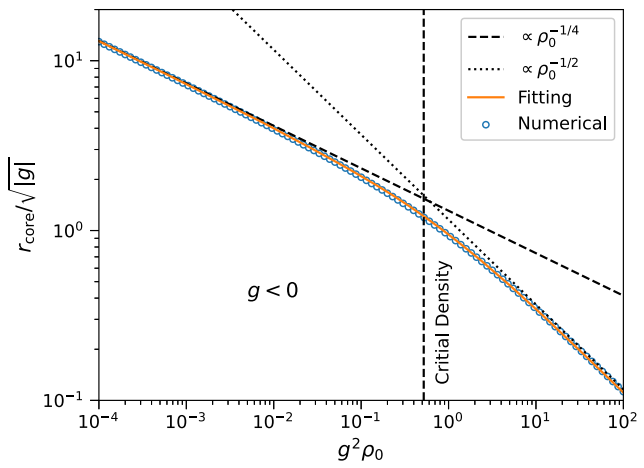

FIG. 17. Core radius of boson star with attractive self-interactions ($g < 0$) as a function of the central density. Circles: numeric results. Solid line: fitting function, Eq. (C12).

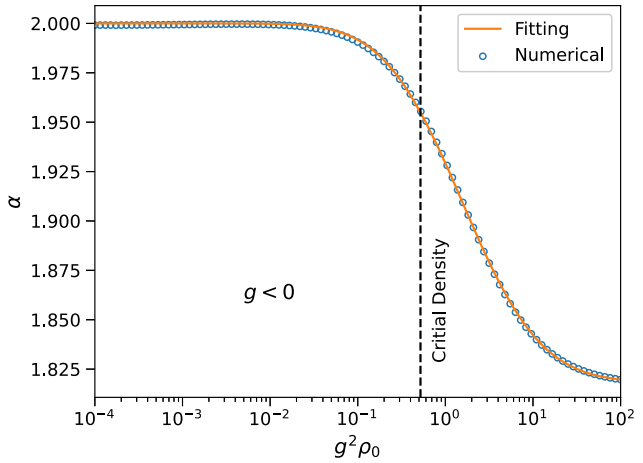

FIG. 18. Parameter α in the fitting formula Eq. (C11) for the case with attractive self-interactions ($g < 0$). Circles: numeric results. Solid line: fitting function, Eq. (C13).

To get the fitting formula for the density profile, we also need to know how the core radius depends on g and ρ_0. Figure 17 shows the core radii of boson stars with different central densities. As can been seen, when $g^2\rho_0 \ll 1$, the core radius $r_{\rm core} \propto \rho_0^{-1/4}$, recovering the relation seen in the case without self-interactions. When $g^2\rho_0 \gg 1$, $r_{\rm core} \propto \rho_0^{-1/2}$. So we assume the core radius has the form

$$r_{\rm core} = 1.308\sqrt{|g|}\left[-\frac{a}{2} + \sqrt{\left(\frac{a}{2}\right)^2 + \frac{1}{g^2\rho_0}}\right]^{1/2}, \quad \text{(C12)}$$

where a is a free parameter needed to be determined by fitting the numerical results. We find the best-fit value of a

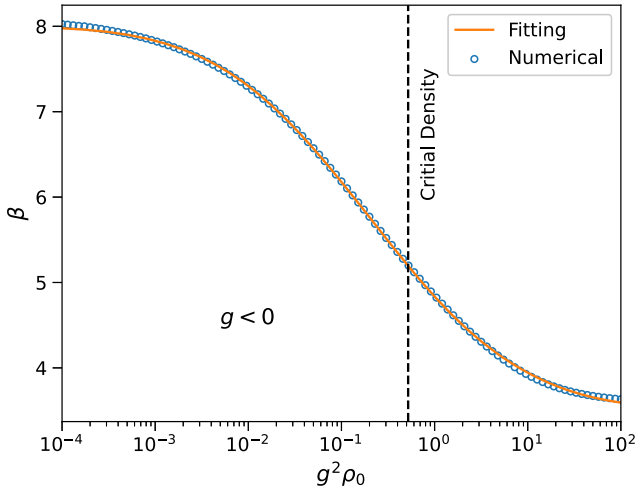

FIG. 19. Parameter β in the fitting formula Eq. (C11) for the case with attractive interactions ($g < 0$) as a function of the central density. Solid line: fitting function, Eq. (C14).

is 1.375. Note that the solution with $g^2\rho > 0.52$ is unstable as discussed previously, but we include all the solutions with $10^{-4} < g^2\rho_0 < 10^2$ in the fitting process so that we can correctly get the transition between two limits: $r_{\rm core} \propto \rho_0^{-1/4}$ and $r_{\rm core} \propto \rho_0^{-1/2}$.

To determine the parameter α and β for each solution, we first fix the core radius using Eq. (C12). Then we fit $r^2\rho(r)$ within the range $0.01r_{\rm core} < r < 5r_{\rm core}$. The best-fit α and β for different $g^2\rho_0$ are shown in Figs. 18 and 19, respectively. We find that the dependence of α and β on $g^2\rho_0$ can be well fit by

$$\alpha = \alpha_a + (2-\alpha_a)\tanh^8[\alpha_b(g^2\rho_0)^{-\alpha_c}], \tag{C13}$$

$$\beta = \beta_a + (8-\beta_a)\tanh^8[\beta_b(g^2\rho_0)^{-\beta_c}]. \tag{C14}$$

The best-fit values for α_i and β_i ($i = a, b, c$) are listed in Table I.

Similarly, we can find the relation between $r_{\rm core}$ and ρ_0 for the case with repulsive self-interactions ($g > 0$). We assume

$$r_{\rm core} = \begin{cases} 1.308\sqrt{|g|}[2+(g^2\rho_0)^{-b}]^{\frac{1}{4b}}, & g^2\rho_0 \le 1.5, \\ c\sqrt{|g|}, & g^2\rho_0 > 1.5, \end{cases} \tag{C15}$$

considering that when $g^2\rho \gg 1$, we have Thomas-Fermi-like solution at small radii

$$\rho(r) = \rho_0 \frac{\sin(r/\sqrt{g})}{r/\sqrt{g}}, \tag{C16}$$

which gives a core radius that is independent of the central density. We find the best-fit $b = 0.710752$, and $c = 1.86543$. Figure 20 shows the fitting formula of $r_{\rm core}$ (solid line) compared with the numerical results (circles).

As in the $g < 0$ case, we also fit $r^2\rho(r)$ within the range $0.01r_{\rm core} < r < 5r_{\rm core}$ to the results obtained from numerical wave function. But we have fixed β at 8. Allowing β to be a free parameter does not improve the fit too much. For the dependence of α on $g^2\rho$ we take the same form as in Eq. (C13). The best-fit α_i are listed in Table I. A comparison between the fitting function of α and the one obtained from numerical results is shown in Fig. 21.[5] We have fitted the soliton density for $10^{-4} < g^2\rho < 10$, but we note that Eq. (C11) cannot well describe the soliton density at very small radii when $g^2\rho \gtrsim 1$. In those cases, the Thomas-Fermi-like solution equation (C16) is more accurate at $r < r_{\rm core}$.

For other approximate soliton solutions with and without self-interactions, see [88,89].

TABLE I. Best-fit parameters for the soliton density with attractive ($g < 0$) and repulsive ($g > 0$) self-interactions.

	$g < 0$	$g > 0$
α_a	1.81823	3.96849
α_b	1.73925	2.11238
α_c	0.22478	0.143883
β_a	3.48601	
β_b	1.29355	$\beta = 8$
β_c	0.122718	

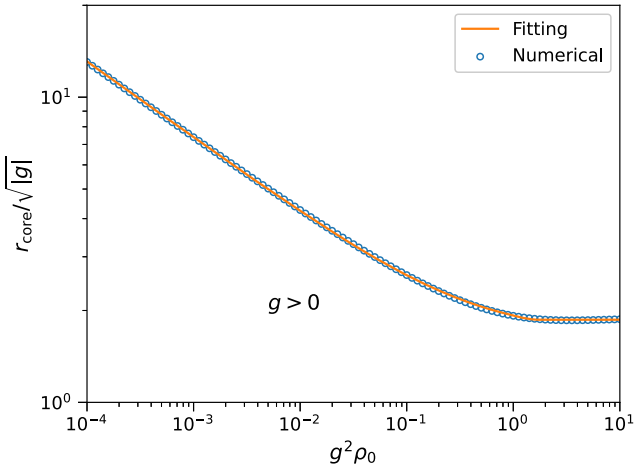

FIG. 20. Core radius of boson star with repulsive self-interactions ($g > 0$) as a function of the central density. Circles: numeric results. Solid line: fitting function, Eq. (C15).

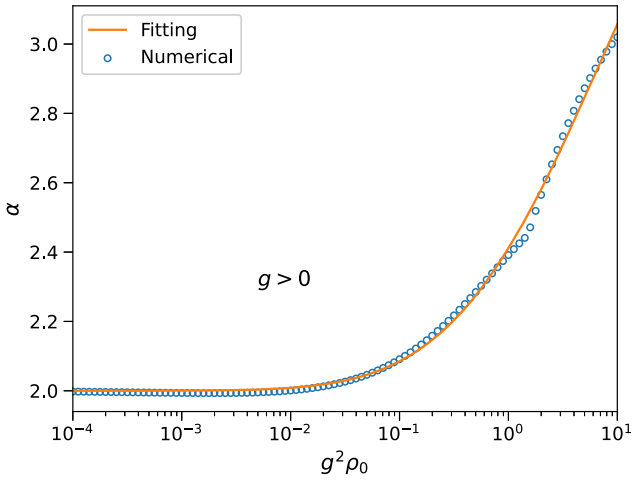

FIG. 21. Parameter α in the fitting formula Eq. (C11) for the case with repulsive self-interactions ($g > 0$) as a function of the central density. Circles: numeric results. Solid line: fitting function, Eq. (C13).

[5]When we derive α for each soliton solution by fitting Eq. (C11) to the numerical results, we fix the core radius using Eq. (C15) which is not smooth at $g^2\rho_0 = 1.5$. So the values of α with respect to $g^2\rho_0$ we obtain (circles) has a small fluctuation around that density.

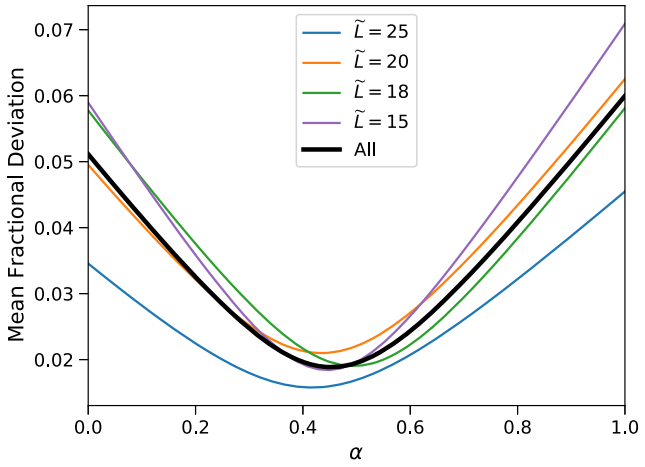

FIG. 22. Mean fractional deviation from the fitting formula $\tilde{M}_{*,\mathrm{sat}} \propto \tilde{N}^{\alpha}$. The colored lines show the results from simulations grouped by box size, while the black line shows the results combing all simulations.

APPENDIX D: BOSON STAR MASS AT SATURATION TIME

As is shown in Sec. III A 2, bosons can condense into boson star in a minicluster through long-range gravitational interaction. The growth of boson star saturates when the virial velocity of the star equals to the virial velocity of the minicluster. The mass of boson star at saturation time is proportional to $\tilde{N}^{\alpha}$, where $\tilde{N}$ is the total mass in the simulation box. To find the best-fit parameter α, we define the mean fractional deviation σ_{α} as

$$\sigma_{\alpha}^2 = \frac{1}{N_{\mathrm{bin}}} \sum_i \left(\frac{\tilde{M}_{*,i}(\alpha) - \tilde{M}_{*,\mathrm{mean}}(\alpha)}{\tilde{M}_{*,\mathrm{mean}}(\alpha)} \right)^2. \tag{D1}$$

Here $\tilde{M}_{*,i}(\alpha)$ is the boson star mass normalized by $\tilde{N}^{\alpha}$, $\tilde{M}_{*,\mathrm{mean}}(\alpha)$ is the mean value within a specific time bin (see Fig. 3 for more explanations). We only include the data at $t/\tau_{\mathrm{gravity}} > 20$. Figure 22 shows σ_{α} calculated for each set of simulations with the same box size (colored lines) and the combined σ_{α} including all simulations (black line). We find that the mean fractional deviation is minimized at $\alpha \sim 0.45$, which is close to the value we would expect from the core mass-halo mass relation found in previous studies [38], i.e. $\tilde{M}_{*} \propto \tilde{M}_{\mathrm{halo}}^{1/3} \propto \tilde{N}^{1/3}$.

APPENDIX E: CONDENSATION TIME FOR GRAVITATIONAL AND SELF-INTERACTIONS

The transport cross section for self-interaction and gravity are $\sigma_{\mathrm{self}} = m^2 g^2/(2\pi)$ and $\sigma_{\mathrm{gravity}} \sim 8\pi(mG)^2\Lambda/v^4$, respectively [40]. The ratio of condensation time of self-interaction to gravity can be written as

$$\frac{\tau_{\mathrm{gravity}}}{\tau_{\mathrm{self}}} \sim \frac{\sigma_{\mathrm{self}}}{\sigma_{\mathrm{gravity}}} \sim \frac{g^2 v^4}{16\pi^2 G^2 \log(mvL)}, \tag{E1}$$

where τ_{self} is the condensation time due to self-interaction. Using Eq. (E1), we can estimate the effect of self-interaction and gravity on the condensation of boson stars. For example, for a system of typical QCD axions with $v \approx 10^{-10}$, and decay constant $f_a \approx 10^{11}$ GeV ($g = -\frac{1}{8f_a^2}$), we have $\tau_{\mathrm{gravity}}/\tau_{\mathrm{self}} \ll 1$, thus gravity plays a much more important role in the condensation process.

Recently, Kay Kirkpatrick *et al.* [70] argue that the relaxation rate due to self-interaction is proportional to $|g|$ rather than g^2, suggesting a much shorter condensation time for self-interaction compared to the one reported by other literature. Further simulations are needed to verify this. However, for typical QCD axions gravity still dominates the condensation process.

[1] N. Aghanim *et al.* (Planck Collaboration), Planck 2018 results. VI. Cosmological parameters, Astron. Astrophys. **641**, A6 (2020).
[2] M. Dine and W. Fischler, The Not So Harmless Axion, Phys. Lett. **120B**, 137 (1983).
[3] A. Surez, V. H. Robles, and T. Matos, A review on the scalar Field/Bose-Einstein condensate dark matter model, Astrophys. Space Sci. Proc. **38**, 107 (2014).
[4] J. Preskill, M. B. Wise, and F. Wilczek, Cosmology of the invisible axion, Phys. Lett. **120B**, 127 (1983).
[5] L. Abbott and P. Sikivie, A cosmological bound on the invisible axion, Phys. Lett. **120B**, 133 (1983).
[6] A. H. Guth, M. P. Hertzberg, and C. Prescod-Weinstein, Do dark matter axions form a condensate with long-range correlation?, Phys. Rev. D **92**, 103513 (2015).
[7] L. M. Widrow and N. Kaiser, Using the schroedinger equation to simulate collisionless matter, Astrophys. J. Lett. **416**, L71 (1993).
[8] C. Uhlemann, M. Kopp, and T. Haugg, Schrödinger method as N-body double and UV completion of dust, Phys. Rev. D **90**, 023517 (2014).
[9] P. Sikivie, Axion cosmology, Lect. Notes Phys. **741**, 19 (2008).

[10] A. Arvanitaki, S. Dimopoulos, S. Dubovsky, N. Kaloper, and J. March-Russell, String Axiverse, Phys. Rev. D **81**, 123530 (2010).
[11] D. G. Levkov, A. G. Panin, and I. I. Tkachev, Relativistic Axions from Collapsing Bose Stars, Phys. Rev. Lett. **118**, 011301 (2017).
[12] R. D. Peccei and H. R. Quinn, *CP* Conservation in the Presence of Instantons, Phys. Rev. Lett. **38**, 1440 (1977).
[13] S. Weinberg, A New Light Boson?, Phys. Rev. Lett. **40**, 223 (1978).
[14] F. Wilczek, Problem of Strong p and t Invariance in the Presence of Instantons, Phys. Rev. Lett. **40**, 279 (1978).
[15] J. E. Kim, Weak Interaction Singlet and Strong *CP* Invariance, Phys. Rev. Lett. **43**, 103 (1979).
[16] M. A. Shifman, A. Vainshtein, and V. I. Zakharov, Can confinement ensure natural *CP* invariance of strong interactions?, Nucl. Phys. **B166**, 493 (1980).
[17] A. Zhitnitsky, On possible suppression of the axion hadron interactions. (In Russian), Sov. J. Nucl. Phys. **31**, 260 (1980).
[18] M. Dine, W. Fischler, and M. Srednicki, A simple solution to the strong *CP* problem with a harmless axion, Phys. Lett. **104B**, 199 (1981).
[19] A. Arvanitaki, M. Baryakhtar, and X. Huang, Discovering the QCD axion with black holes and gravitational waves, Phys. Rev. D **91**, 084011 (2015).
[20] A. Payez, C. Evoli, T. Fischer, M. Giannotti, A. Mirizzi, and A. Ringwald, Revisiting the SN1987A gamma-ray limit on ultralight axion-like particles, J. Cosmol. Astropart. Phys. 02 (2015) 006.
[21] D. J. E. Marsh, Axion cosmology, Phys. Rep. **643**, 1 (2016).
[22] M. Tanabashi *et al.* (Particle Data Group Collaboration), Review of particle physics, Phys. Rev. D **98**, 030001 (2018).
[23] L. D. Luzio, M. Giannotti, E. Nardi, and L. Visinelli, The landscape of QCD axion models, Phys. Rep. **870**, 1 (2020).
[24] W. H. Press, B. S. Ryden, and D. N. Spergel, Single Mechanism for Generating Large-Scale Structure and Providing Dark Missing Matter, Phys. Rev. Lett. **64**, 1084 (1990).
[25] V. Sahni and L. Wang, New cosmological model of quintessence and dark matter, Phys. Rev. D **62**, 103517 (2000).
[26] W. Hu, R. Barkana, and A. Gruzinov, Cold and Fuzzy Dark Matter, Phys. Rev. Lett. **85**, 1158 (2000).
[27] P. J. E. Peebles, Fluid dark matter, Astrophys. J. Lett. **534**, L127 (2000).
[28] D. J. E. Marsh and A.-R. Pop, Axion dark matter, solitons and the cusp-core problem, Mon. Not. R. Astron. Soc. **451**, 2479 (2015).
[29] L. Hui, J. P. Ostriker, S. Tremaine, and E. Witten, Ultralight scalars as cosmological dark matter, Phys. Rev. D **95**, 043541 (2017).
[30] E. Seidel and W.-M. Suen, Dynamical evolution of boson stars: Perturbing the ground state, Phys. Rev. D **42**, 384 (1990).
[31] D. J. Kaup, Klein-Gordon Geon, Phys. Rev. **172**, 1331 (1968).
[32] R. Ruffini and S. Bonazzola, Systems of self-gravitating particles in general relativity and the concept of an equation of state, Phys. Rev. **187**, 1767 (1969).
[33] E. Seidel and W.-M. Suen, Formation of Solitonic Stars Through Gravitational Cooling, Phys. Rev. Lett. **72**, 2516 (1994).
[34] M. Alcubierre, R. Becerril, S. F. Guzman, T. Matos, D. Nunez, and L. A. Urena-Lopez, Numerical studies of Phi**2 oscillatons, Classical Quantum Gravity **20**, 2883 (2003).
[35] T. Helfer, D. J. E. Marsh, K. Clough, M. Fairbairn, E. A. Lim, and R. Becerril, Black hole formation from axion stars, J. Cosmol. Astropart. Phys. 03 (2017) 055.
[36] A. R. Liddle and M. S. Madsen, The structure and formation of boson stars, Int. J. Mod. Phys. D **01**, 101 (1992).
[37] H.-Y. Schive, T. Chiueh, and T. Broadhurst, Cosmic structure as the quantum interference of a coherent dark wave, Nat. Phys. **10**, 496 (2014).
[38] H.-Y. Schive, M.-H. Liao, T.-P. Woo, S.-K. Wong, T. Chiueh, T. Broadhurst, and W.-Y. P. Hwang, Understanding the Core-Halo Relation of Quantum Wave Dark Matter from 3D Simulations, Phys. Rev. Lett. **113**, 261302 (2014).
[39] B. Schwabe, J. C. Niemeyer, and J. F. Engels, Simulations of solitonic core mergers in ultralight axion dark matter cosmologies, Phys. Rev. D **94**, 043513 (2016).
[40] D. G. Levkov, A. G. Panin, and I. I. Tkachev, Gravitational Bose-Einstein Condensation in the Kinetic Regime, Phys. Rev. Lett. **121**, 151301 (2018).
[41] J. Y. Widdicombe, T. Helfer, D. J. E. Marsh, and E. A. Lim, Formation of relativistic axion stars, J. Cosmol. Astropart. Phys. 10 (2018) 005.
[42] B. Eggemeier and J. C. Niemeyer, Formation and mass growth of axion stars in axion miniclusters, Phys. Rev. D **100**, 063528 (2019).
[43] C. A. OHare and A. M. Green, Axion astronomy with microwave cavity experiments, Phys. Rev. D **95**, 063017 (2017).
[44] D. J. Kimball, D. Budker, J. Eby, M. Pospelov, S. Pustelny, T. Scholtes, Y. Stadnik, A. Weis, and A. Wickenbrock, Searching for axion stars and q -balls with a terrestrial magnetometer network, Phys. Rev. D **97**, 043002 (2018).
[45] G. F. Giudice, M. McCullough, and A. Urbano, Hunting for dark particles with gravitational waves, J. Cosmol. Astropart. Phys. 10 (2016) 001.
[46] T. Helfer, E. A. Lim, M. A. Garcia, and M. A. Amin, Gravitational wave emission from collisions of compact scalar solitons, Phys. Rev. D **99**, 044046 (2019).
[47] S. Bird, I. Cholis, J. B. Muñoz, Y. Ali-Haïmoud, M. Kamionkowski, E. D. Kovetz, A. Raccanelli, and A. G. Riess, Did LIGO Detect Dark Matter?, Phys. Rev. Lett. **116**, 201301 (2016).
[48] X.-P. Wu, T. Chiueh, L.-Z. Fang, and Y.-J. Xue, A comparison of different cluster mass estimates: Consistency or discrepancy ?, Mon. Not. R. Astron. Soc. **301**, 861 (1998).
[49] G. Hinshaw *et al.* (WMAP Collaboration), Five-year Wilkinson microwave anisotropy probe (WMAP) observations: Data processing, sky maps, and basic results, Astrophys. J. Suppl. Ser. **180**, 225 (2009).
[50] P. Natarajan *et al.*, Mapping substructure in the HST frontier fields cluster lenses and in cosmological simulations, Mon. Not. R. Astron. Soc. **468**, 1962 (2017).

[51] A. Refregier, Weak Gravitational Lensing by Large-Scale Structure, Annu. Rev. Astron. Astrophys. **41**, 645 (2003).
[52] G. Bertone and D. Merritt, Dark matter dynamics and indirect detection, Mod. Phys. Lett. A **20**, 1021 (2005).
[53] D. Merritt, Dark matter at the centers of galaxies, arXiv:1001.3706.
[54] J. Ellis, R. A. Flores, K. Freese, S. Ritz, D. Seckel, and J. Silk, Cosmic ray constraints on the annihilations of relic particles in the galactic halo, Phys. Lett. B **214**, 403 (1988).
[55] D. G. Levkov, A. G. Panin, and I. I. Tkachev, Relativistic Axions from Collapsing Bose Stars, Phys. Rev. Lett. **118**, 011301 (2017).
[56] B. Fornberg, The pseudospectral method: Comparisons with finite differences for the elastic wave equation, Geophysics **52**, 483 (1987).
[57] J. Magaa and T. Matos, A brief review of the scalar field dark matter model, J. Phys. Conf. Ser. **378**, 012012 (2012).
[58] M. A. Amin and P. Mocz, Formation, gravitational clustering, and interactions of nonrelativistic solitons in an expanding universe, Phys. Rev. D **100**, 063507 (2019).
[59] D. J. E. Marsh and J. C. Niemeyer, Strong Constraints on Fuzzy Dark Matter from Ultrafaint Dwarf Galaxy Eridanus II, Phys. Rev. Lett. **123**, 051103 (2019).
[60] N. Bar, D. Blas, K. Blum, and S. Sibiryakov, Galactic rotation curves versus ultralight dark matter: Implications of the soliton-host halo relation, Phys. Rev. D **98**, 083027 (2018).
[61] Z. Li, J. Shen, and H.-Y. Schive, Testing the prediction of fuzzy dark matter theory in the Milky Way center, Astrophys. J. **889**, 88 (2020).
[62] A. Hook, Y. Kahn, B. R. Safdi, and Z. Sun, Radio Signals from Axion Dark Matter Conversion in Neutron Star Magnetospheres, Phys. Rev. Lett. **121**, 241102 (2018).
[63] D. F. J. Kimball, D. Budker, J. Eby, M. Pospelov, S. Pustelny, T. Scholtes, Y. V. Stadnik, A. Weis, and A. Wickenbrock, Searching for axion stars and Q-balls with a terrestrial magnetometer network, Phys. Rev. D **97**, 043002 (2018).
[64] G. F. Giudice, M. McCullough, and A. Urbano, Hunting for dark particles with gravitational waves, J. Cosmol. Astropart. Phys. 10 (2016) 001.
[65] P. H. Chavanis and L. Delfini, Mass-radius relation of Newtonian self-gravitating Bose-Einstein condensates with short-range interactions: II. Numerical results, Phys. Rev. D **84**, 043532 (2011).
[66] J. Eby, C. Kouvaris, N. G. Nielsen, and L. Wijewardhana, Boson stars from self-interacting dark matter, J. High Energy Phys. 02 (2016) 028.
[67] X. Du, B. Schwabe, J. C. Niemeyer, and D. Bürger, Tidal disruption of fuzzy dark matter subhalo cores, Phys. Rev. D **97**, 063507 (2018).
[68] P. Mocz, M. Vogelsberger, V. Robles, J. Zavala, M. Boylan-Kolchin, and L. Hernquist, Galaxy Formation with BECDM: I. Turbulence and relaxation of idealised haloes, Mon. Not. R. Astron. Soc. **471**, 4559 (2017).
[69] M. Khlopov, B. Malomed, and I. Zeldovich, Gravitational instability of scalar fields and formation of primordial black holes, Mon. Not. R. Astron. Soc. **215**, 575 (1985).
[70] K. Kirkpatrick, A. E. Mirasola, and C. Prescod-Weinstein, Relaxation times for Bose-Einstein condensation in axion miniclusters, Phys. Rev. D **102**, 103012 (2020).
[71] E. W. Kolb and I. I. Tkachev, Axion Miniclusters and Bose Stars, Phys. Rev. Lett. **71**, 3051 (1993).
[72] E. W. Kolb and I. I. Tkachev, Nonlinear axion dynamics and formation of cosmological pseudosolitons, Phys. Rev. D **49**, 5040 (1994).
[73] E. W. Kolb and I. I. Tkachev, Femtolensing and Picolensing by Axion Miniclusters, Astrophys. J. Lett. **460**, L25 (1996).
[74] P.-H. Chavanis, Mass-radius relation of Newtonian self-gravitating Bose-Einstein condensates with short-range interactions. I. Analytical results, Phys. Rev. D **84**, 043531 (2011).
[75] P.-H. Chavanis, Collapse of a self-gravitating Bose-Einstein condensate with attractive self-interaction, Phys. Rev. D **94**, 083007 (2016).
[76] J. A. R. Cembranos, A. L. Maroto, S. J. N. Jareo, and H. Villarrubia-Rojo, Constraints on anharmonic corrections of fuzzy dark matter, J. High Energy Phys. 08 (2018) 073.
[77] J. Veltmaat, J. C. Niemeyer, and B. Schwabe, Formation and structure of ultralight bosonic dark matter halos, Phys. Rev. D **98**, 043509 (2018).
[78] P.-H. Chavanis, Growth of perturbations in an expanding universe with Bose-Einstein condensate dark matter, Astron. Astrophys. **537**, A127 (2012).
[79] V. Desjacques, A. Kehagias, and A. Riotto, Impact of ultralight axion self-interactions on the large scale structure of the Universe, Phys. Rev. D **97**, 023529 (2018).
[80] J. C. Niemeyer and R. Easther, Inflaton clusters and inflaton stars, J. Cosmol. Astropart. Phys. 07 (2020) 030.
[81] X. Du, C. Behrens, J. C. Niemeyer, and B. Schwabe, Core-halo mass relation of ultralight axion dark matter from merger history, Phys. Rev. D **95**, 043519 (2017).
[82] N. Musoke, S. Hotchkiss, and R. Easther, Lighting the Dark: Evolution of the Postinflationary Universe, Phys. Rev. Lett. **124**, 061301 (2020).
[83] K. Clough, T. Dietrich, and J. C. Niemeyer, Axion star collisions with black holes and neutron stars in full 3D numerical relativity, Phys. Rev. D **98**, 083020 (2018).
[84] https://docs.nvidia.com/cuda/cufft/index.html.
[85] R. I. McLachlan, On the numerical integration of ordinary differential equations by symmetric composition methods, SIAM J. Sci. Comput. **16**, 151 (1995).
[86] S. A. Chin, Forward and non-forward symplectic integrators in solving classical dynamics problems, arXiv:0704.3273.
[87] T.-P. Woo and T. Chiueh, High-resolution simulation on structure formation with extremely light bosonic dark matter, Astrophys. J. **697**, 850 (2009).
[88] F. Kling and A. Rajaraman, Towards an analytic construction of the wavefunction of boson stars, Phys. Rev. D **96**, 044039 (2017).
[89] F. Kling and A. Rajaraman, Profiles of boson stars with self-interactions, Phys. Rev. D **97**, 063012 (2018).